Measurement 79 (2016) 53–65

Contents lists available at ScienceDirect

Measurement

journal homepage: www.elsevier.com/locate/measurement

Offshore wind turbine blades measurement using Coherent Laser Radar

Jeremy Talbot [a], Qing Wang [a,*], Neil Brady [b], Roger Holden [b]

[a] School of Engineering and Computing Sciences, Durham University, DH1 3LE, UK
[b] Nikon Metrology UK Ltd, Staffordshire B77 5ES, UK

ARTICLE INFO

Article history:
Received 18 March 2015
Received in revised form 10 October 2015
Accepted 22 October 2015
Available online 30 October 2015

Keywords:
B-spline
Coherent Laser Radar (CLR)
Data alignment
Degrees of Freedom (DoF)
Transformation
Wind turbine blades

ABSTRACT

To maximize aerodynamic efficiency, large-scale offshore wind turbine blades require inspection during the production stage to ensure strict tolerance requirements are met. During production, the blade is fixed at the root, restricting movement in the *Z* direction. *X*, *Y*, *Rx*, *Ry* and *Rz* remain unconstrained causing blade flex due to gravity. This deforms the blade away from the theoretical CAD blade location, causing measurement results that do not accurately represent the blade profile. Measurement error can be minimized using rigorous B-spline data alignment. Such alignment compensates for blade flex by varying the constrained Degrees of Freedom (DoF), and provides manufacturers with confidence in the design process. This paper used Coherent Laser Radar and Spatial Analyzer to establish the optimal constrained DoF variation, giving the most accurate data alignment solution. Of the constraints investigated, the optimal data transformation solution was found with a double B-spline alignment method, whilst constraining movement in *Y*, *Z* and *Ry*.

1. Introduction

Changing climate and increasing awareness of environmental issues in recent years has resulted in a huge increase in the use of low-carbon technologies, particularly wind energy. The contribution of electricity generation from renewable energy has increased from 2.6% in 2000 to 11.5% in 2012 [1] (a target of 15% is set for 2020). Of this renewable energy, 47% is produced by wind power (29% onshore and 18% offshore). This is expected to increase further still.

To produce a large quantity of energy (usually between 1.5 and 4 MW), wind turbines must be extremely large and are therefore subject to strong wind loads. To ensure blades can survive these high wind loads whilst remaining lightweight, they are manufactured with an internal frame supporting an outer shell made from reinforced plastics [2,3].

To maximize aerodynamic efficiency, turbine blades must satisfy extremely tight tolerances and are therefore inspected during manufacture. However, inspection shows a divergence from the theoretical blade design due to shrinkage of the reinforced plastic during manufacture and blade flex under its own weight. Hence, minimizing the three-dimensional (3-D) measurement error during blade inspection is imperative. It provides manufacturers with confidence in the design process; highlighting areas of the blade that deviate away from the CAD model allows the production of more aerodynamically efficient blades.

If flexible, deformation of a turbine blade (or any structure) can consist of up to six Degrees of Freedom (DoF): translational (*X*, *Y* and *Z*), and rotational (*Rx*, *Ry* and *Rz*) directions. Fig. 1 shows a typical large-scale wind turbine blade with a reference coordinate frame showing the translational *X*, *Y* and *Z* directions.

* Corresponding author. Tel.: +44 191 334 2381; fax: +44 191 3342408.
E-mail addresses: jtalbot.gcap@gmail.com (J. Talbot), qing.wang@durham.ac.uk (Q. Wang), neil.brady@nikon.com (N. Brady), roger.holden@nikon.com (R. Holden).

http://dx.doi.org/10.1016/j.measurement.2015.10.030
0263-2241/

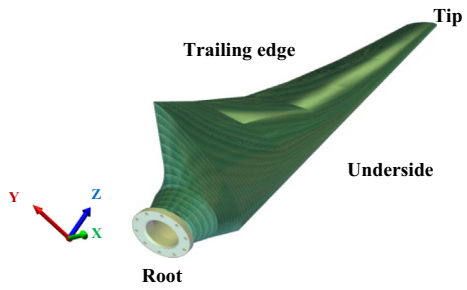

Fig. 1. A typical wind turbine blade. (Blade image by M.A. Homel [4].)

The blade is also free to rotate about the *X*, *Y* and *Z* axes, relating to *Rx*, *Ry* and *Rz* rotational directions.

The inspection of turbine blades compares the measured blade data to nominal point groups on a computer-aided design (CAD) model using data alignment techniques. These techniques transform the measured data using different constrained DoF variations to account for blade flex. The measurement error is minimized by establishing the most accurate DoF constrained data alignment variation.

There are a number of software packages available that can provide a platform for such data alignment including Spatial Analyzer (SA) which was used in this investigation.

Nikon have recently developed a method [5] for inspecting turbine blades using CLR; it is currently in use by Vestas Winds Systems A/S. The method divides a blade into sections using multiple scanner locations to measure the entire blade (six locations are needed for a 60 m blade). The blade is clamped at the root, positioned horizontally with the trailing edge directed upward and supported on a 'tray' half way along the length of the blade. It can be assumed clamping the blade at the root in this manner restricts any movement in the *Z* direction, allowing inspection through five DoF.

An advantage of this method is CLR's unique ability to precisely measure with retroreflective mirrors. Using dedicated mirrors expands the range of sight, enabling the measurement of difficult-to-access areas such as the underside of the blade, allowing accurate inspection of the entire blade.

The data alignment technique currently used by Nikon implements *Z*, *Rx*, and *Ry* constraints, allowing movement in the *X*, *Y* and *Rz* directions. As this method has only recently been developed, very little experimental evaluation has been carried out; DoF constraint variations have been chosen using trial and error. This is especially true of the use of mirrors in CLR. The method therefore requires validation before it becomes common practice industrially.

This research investigates the Nikon inspection method and continues the work that demonstrated a data alignment solution based on a 'D-shaped', semi-circular blade design [6]. This research uses a similar method to that in [6] on a more complex, realistic blade profile which necessitates the use of mirrors.

Measurement error is minimized by evaluating each DoF constraint variation to determine the optimal data alignment solution. The results will propose the most accurate and time-efficient data alignment measurement solution for the large-scale metrology of wind turbine blades using CLR technology. Additionally, effects of using a mirror on measurement accuracy are investigated.

2. Theory

2.1. Coherent Laser Radar technology

There are a number of metrology techniques available today [7] capable of measuring structures on a large-scale. The high accuracy of Coherent Laser Radar (CLR) along with its non-contact technology, application to large-scale structures, speed and portability are all key features shown in Fig. 2 which make CLR the optimal metrology technique for turbine blade inspection.

Contact metrology typically uses touch probes in contact with a surface to measure 3-D coordinates. Historically, contact devices have been able to measure surfaces to a higher accuracy than that of non-contact devices. Nikon's CMM contact devices can measure a 3-D point to a volumetric accuracy of 1.8 μm [9]. More recently, non-contact technology has advanced and is now capable of measuring to a high accuracy [10].

There are several disadvantages to using touch probes for contact methods. They are slow, require an operator, are difficult to manipulate and must be in contact with the surface which could potentially deform the measurement surface and requires the calculation of touch probe radius offsets [11]. Using touch probes for large-scale applications would therefore be extremely time-consuming; CLR can achieve a 90% inspection cycle time reduction compared with alternative contact methods [12].

Due to the large size of turbine blades, multiple CLR scanner locations are needed to inspect a complete blade. However, CLR scanners are portable and the method is fast. The CLR equipment used in this piece of research is Nikon's FM CLR Scanner (LR 200) [13], which is capable of inspecting up to 2000 points per second with a range of 50 m.

The scanner works by emitting a linear infrared laser beam onto the measurement surface and recapturing a portion of the reflected light. The laser signal's strength and ability to accurately focus at any distance from the scanner is maximized with an adjustable, large-aperture fixing [8]. Heterodyne detection [14] of the reflected beam mixed coherently with a controlled reference signal of calibrated wavelength (Fig. 3) can precisely measure the change in frequency (Δf) and the change in time (Δt) of the waveform.

The absolute range is determined using frequency modulation as shown in Eq. (1) [8].

$$\text{Range} = \frac{\Delta f}{0.667} \quad (\mu, \text{microns}) \tag{1}$$

Calculating the measurement points using frequency modulation produces a more accurate reading than if using light modulation shown in Eq. (2) [8]. At a distance of 2 m

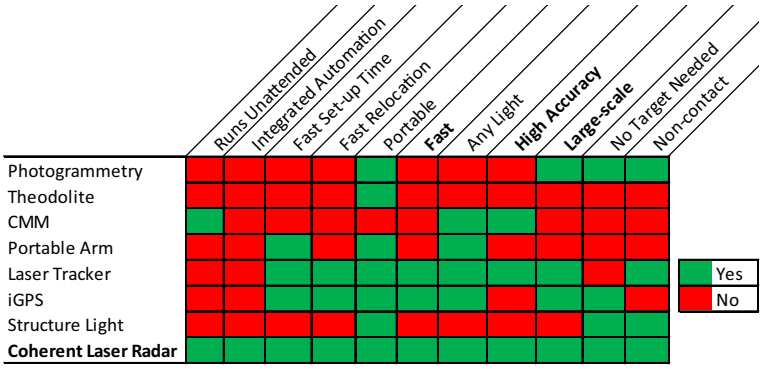

Fig. 2. Comparison of various metrology techniques across wind turbine blade inspection criteria [8].

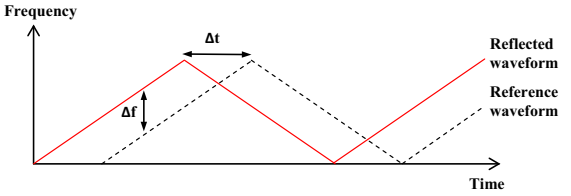

Fig. 3. Comparison of the reflected laser signal with the controlled reference signal. Δf can be calculated due to a base frequency 200 THz and a fixed wavelength of 1500 nm [8].

(similar to that used during this research), a 3-D measurement can be calculated using frequency modulation to within 24 μm [13].

$$\text{Range} = \frac{\Delta t \times c}{2} \quad (\mu\text{m}) \tag{2}$$

where c is the speed of light and 1 μm = 6.7×10^{-15} s.

Reliance on frequency shift means the scanner is largely insensitive to surface reflection and therefore only needs to recapture about 1% of the reflected beam [15]. This allows the inspection of composite materials such as turbine blade outer shells in any light. It also reduces human error when using tooling balls. Tooling balls used commonly as alignment reference points due to their geometrical precision for CAD alignment.

The laser beam is directed using a scan mirror mounted on a two-axis-gimbal shown in Fig. 4, allowing movement through 360° azimuth (Az) and 120° elevation (El) to determine the point range (Rg).

To determine the point range, the scanner measures a distance and two angles. The scanner can measure the X and Y values (angles) precisely using probes within the two-axis movement mechanism. The Z value (range) on the other hand is determined by processing the reflected beams and is therefore less accurate [10]. Nikon [16], state that CLR has an angle uncertainty of 6.8 μm/m compared to a range uncertainty of 10 μm/m + 2.5 μm/m.

The range accuracy characteristics were also demonstrated using the flip test within SA. Ten tooling balls were measured and errors (i.e. magnitude away from the theoretical point location) for azimuth, elevation and range were recorded; an absolute average was calculated, shown in Fig. 5.

Fig. 5 shows that errors in range measurement are 2.45 and 7.71 times greater than azimuth and elevation measurement errors respectively.

There are various uncertainties associated with CLR because of assumptions compensating for environmental factors [15]. In this investigation, it was assumed that the laser beam travelled in a straight line [17]. This assumes that: the temperature was uniform across the measurement volume, the air refraction index was constant and effects due to air turbulence from noise vibrations and other mechanical instabilities were negligible and therefore did not affect the laser beam path.

These assumptions can be made in this investigation because measurements were taken from a 2 m distance; environmental factors would therefore be insignificant.

2.2. Mirrors

It was observed that on the underside of the blade where the laser beam was near tangential to the blade

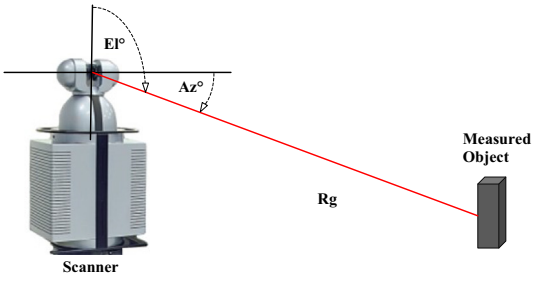

Fig. 4. CLR scanner showing azimuth, elevation and range measurement capabilities.

	Azimuth	Elevation	Range
Average (mm)	0.0022	0.0007	0.0054

Fig. 5. Absolute average (in mm) of measurement errors in azimuth, elevation and range.

surface (i.e. an incidence angle close to 90°), CLR was unable to focus precisely on nominal points, causing measurements to fail.

CLR has a unique ability to measure precisely using mirrors, increasing the available area of vision. This allows measurement around corners and of difficult-to-access areas such as the underside of the blade. Hence, the entire blade profile perimeter can be measured. The micron-polished nickel-plated aluminium mirror used in this investigation was circular with a diameter of 15 cm. Surface nickel plating minimizes the effect of temperature change on the metal as well as improving durability and resistance to scratching, whilst the polished finish creates an extremely smooth surface, reducing beam scatter.

The CLR laser beam is transmitted at a wavelength of 1500 nm. At this wavelength, Laser Beam Products [18] have shown that protected aluminium mirrors offer close to 92% reflectivity. In this investigation, measuring using the mirror required the laser beam to be reflected twice, resulting in an overall reflectivity of ~84.64%. It is suggested that at wavelengths above 700 nm, gold or silver coatings should be used as opposed to nickel [18]. However these are not concerns as CLR needs only 1% reflectivity to operate.

Such a mirror can be challenging and time-consuming to align as there is no well-defined axis. Mirrors were traditionally aligned by measuring the angle normal to the mirrored surface with auto-collimating theodolites [19].

A simpler method of aligning the mirror plane within SA uses a tooling ball. The actual position of the tooling ball is measured normally. This fixed location allows an image of the same tooling ball to be measured using the mirror. With the two measurements, the mirror is determined as the plane halfway between the two points shown in Fig. 6 [20]; where Δa and Δb are the tooling ball uncertainties in the normal and perpendicular directions to the mirror plane, L is the length between the actual and apparent tooling ball positions and U is the uncertainty in the direction of the flat mirror to its normal.

The uncertainty in the direction of the mirror can be determined using Eq. (3).

$$U = \frac{\sqrt{\Delta a_1^2 + \Delta a_2^2}}{L} \tag{3}$$

Uncertainty is therefore greater when the tooling ball is closer to the mirror since L has decreased.

The complex nature of the blade profile and the small mirror size means the laser is only reflected to small sections of the blade. For each experiment configuration, multiple mirror locations were therefore required to inspect the underside of the blade.

The mirror was adjusted using trial and error (which was time-consuming) in order to maximize the number of points that could be measured. It was especially difficult to align the mirror when simulating large offsets as the reference points often fell outside the mirror's line of sight, resulting in failed measurements.

There are two main variables that can affect measurement accuracy when using mirrors: the angle of incidence between the mirror and the laser beam, and the distance away from the mirror.

It was found that a mirror can be used within an acceptable accuracy at an angle of incidence below 50° [21]. A 10° incidence angle yields an uncertainty of less than 3 arc-sec (0.0008°). Although still capable of using the mirror at an angle of incidence of 80°, at angles above 50° the uncertainty increases with incidence angle.

Similarly, at distances less than ~15 m, [21] shows a measurement uncertainty of ±5 arc-sec (0.0014°), which is an acceptable accuracy. However, beyond 15 m, the uncertainty increases with distance.

Uncertainty due to mirror distance was investigated by varying the distance of the mirror away from the blade; ten measurement points were investigated on the underside of the blade and averaged, shown in Fig. 7.

Although the 1 m mirror position appears the most accurate, it must be discounted as CLR was only capable of measuring one out of ten nominal points. Beyond 1 m, CLR was unable to measure any points.

Fig. 7 shows that using a mirror increases measurement accuracy by 29.7% for points on the underside of the blade. It was found that varying the mirror distance below 1 m from the blade did not have an effect on measurement accuracy.

During this investigation, the mirror was used in positions less than 1 m away from the blade whilst the angles of incidence were kept below 50°. Measurements could therefore be made with confidence.

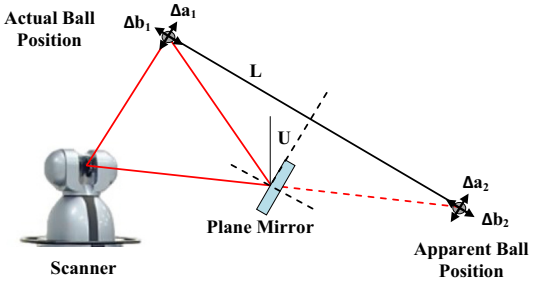

Fig. 6. Tooling ball alignment, needed in order to create a mirror plane in SA [20].

	Mirror distance from blade (m)				
	No Mirror	0.25	0.5	0.75	1
Average point variation (mm)	5.59	3.93	3.93	3.92	3.26

Fig. 7. Average (in mm) variation between measured points and the nominal points on the underside of the blade at different mirror distances away from the blade.

2.3. Spatial Analyzer

There are a number of software packages compatible with CLR, such as Spatial Analyzer and Polyworks. Both of them are highly flexible, instrument-independent, and can be used to develop and deploy automatic inspection processes or guided operator-driven workflows for effective shop floor operations. However this research was carried out using SA. SA is a traceable 3-D graphical software platform [22] that can be used in combination with CLR to manipulate and analyze the measured data in relation to a CAD model.

SA is capable of using multiple scanner locations to inspect the full span of a wind turbine blade. This is achieved using the Unified Spatial Metrology Network (USMN) [23] feature in SA which complies with the Guide to the expression of Uncertainty in Measurement (GUM) [24]. It accurately combines numerous measurement scanners (or relocates a single scanner) throughout the measurement volume. A single coordinate frame is created from the individual coordinate frames from each scanner's data set. Known points along the blade act as an alignment reference for each scanner. However, each scanner has measurement uncertainties which must be combined in order to provide a proper uncertainty statement [25].

This investigation used the best-fit transformation function of SA. The transformation reduces measurement errors by minimizing the distance between the measured blade data and a nominal point group defined in CAD. The measured data is transformed towards the nominal set, altering the measured data (including point-to-point distances, surface distances and scanner movements). The change in data is analyzed to determine the effectiveness of each transformation.

The best-fit transformation is based on the Least Squares method [17], a standard approach to the approximate solution of over-determined systems to adjust parameters of a model function to best fit a data set. However, the Least Squares method is sensitive to extreme outliers. At least three data points are required for a best-fit alignment; however using four or more data points significantly increases the transformation accuracy [17].

In addition, SA allows the raw measured data to be fabricated for other DoF constraints, reducing the time required significantly. SA works by converting the measured CLR data into X, Y and Z coordinates. The resulting coordinates have uncertainties relating to the original data (SA claim a 98% confidence in results) due to the conversion model applied [25]. Complex conversion models are therefore needed to accurately represent the new coordinates.

Physical measurement errors occur when algorithms are used to compensate for properties such as material expansion from temperature [17]. Furthermore, errors can arise within algorithms used to generate curve and point geometry.

2.4. Generating curve and point geometry

A nominal point group must be defined on the surface of the CAD model in SA, to act as a measurement reference for CLR. There are several parametric mathematical methods available which can represent curved surfaces, including Non Uniform Rational B-Splines (NURBS) and Bézier curves [26].

NURBS surfaces are a generalization of B-spline and Bézier surfaces; however the B-spline method is a mathematically simplified version of the NURBS method [27]. B-splines have two advantages over Bézier surfaces: Bézier surfaces have a practical limit to the number of control points that can be used and Bézier point evaluation is less efficient [27].

To generate the required nominal points, first a B-spline curve is constructed on the CAD blade surface. SA uses the de Boor B-spline algorithm [28] to generate the approximate curve $F(t)$ shown in Eq. (4); where A_i are the control points and k the order of polynomial sections.

$$F(t) = \sum_{i=0}^{j} A_i N_{i,k}(t) \tag{4}$$

The curve is located by intersecting with a predefined plane and the CAD surface allowing flexible B-spline positioning. CAD surfaces are often constructed in sections, allowing more complex curved surfaces to be modelled. B-splines can be constructed on each section and combined using knot vectors [29]. Although this enhances errors, extremely complex surfaces can be inspected.

Furthermore, the number of B-splines can vary to match the level of inspection detail required. Increasing the number of B-splines however, increases the computational time.

Due to the straight line construction of B-splines, the CAD surface cannot be modelled exactly. Fig. 8 shows the Hausdorff distance [30] between the exact CAD model surface and the approximate B-spline curve.

Once the B-spline is defined, points can be constructed along the curve either by defining the number of nominal points desired or defining point separation. The latter method was used in this investigation, producing a uniform distribution of points, allowing different levels of inspection for each CAD surface. Results increase in accuracy when using more data points, especially where surface gradients are more severe; however this adds to computational time.

To remove errors associated with the straight line construction of B-splines, points require projecting onto the predefined CAD surface, shown in Fig. 8. The projected points can then be automatically measured using CLR.

2.5. Blade flex

The flex (sag and twist) of a 44 m blade due to gravity was simulated using Computational Analysis [6] by

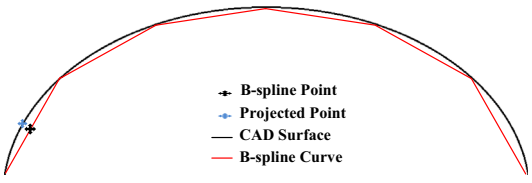

Fig. 8. Difference between CAD surface to B-spline curve and point to projected point [6].

applying a uniform load to the upper surface of the blade profile. The blade was constrained at the root, allowing the blade to move in all directions except *Z*.

The simulation demonstrates the worst case scenario during inspection resulting in an extreme maximum deformation of 5.605 m at the tip of the blade. This displacement relates to a 30° deviation from the *Z* axis (i.e. 30° in *Rz*).

In practice, the blade is positioned trailing edge up and supported by a 'tray'. The blade will therefore undergo less deformation. During testing a tip deviation of ~10 in. (0.254 m) is observed, relating in ~1.5° *Rz* rotation.

In this investigation, the blade test model was offset in *Rx*, *Ry* and *Rz* DoF to simulate severe flex. Optimizing measurement accuracy by determining the optimal constrained DoF variation at maximum flex provides manufacturers with confidence in the measurement capabilities of small, real-life blade deformations observed during testing.

2.6. Data alignment

For inspection, wind turbine blades are constrained at the root, restricting any movement in the *Z* axis. This allows SA to apply best-fit transformations using 5 DoF unconstrained variables; *X*, *Y*, *Rx*, *Ry* and *Rz*. This significantly simplifies data analysis compared with that of transformations in 6 DoF. Allowing movement in 5 DoF produces 32 different constraint variations. The raw measured data is fabricated for each combination and aligned using the best-fit transformation. Each transformation is then analyzed and compared with the other 31 sets of data to determine the optimal DoF constraint variation.

3. Method

3.1. Experimental equipment

The method used in this investigation was designed to test and evaluate the 32 DoF data alignment variations of the blade's constrained movement.

The test piece measured 1.65 m in height and 0.5 m in width. It was a 1:2 size cross-section model based on the Vestas 44 m offshore wind turbine blade section 5.5 m from the root. The test model was mounted on a turntable and a two-axis gimbal and positioned ~2.5 m from the CLR scanner within the metrology laboratory at Durham, shown in Fig. 9. This allowed the blade to be rotated in the *X*, *Y* and *Z* axes.

Blade flex simulated in [6] was replicated in the laboratory using a turntable allowing up to 30° rotation in *Ry* (simulating sag) and a gimbal allowing up to 15° and 20° rotation in *Rx* and *Rz* respectively (simulating twist).

The complex nature of blade profiles means that test models are difficult to manufacture accurately. The test model used in this project was manufactured from plywood and constructed using nails. This method differs significantly from how the actual blade is manufactured. The test model would therefore deviate from the theoretical CAD model in different areas and magnitude to that of a real blade. The test model used in this investigation replicated a real blade profile cross-section more truthfully than that used in [6], reducing measurement error.

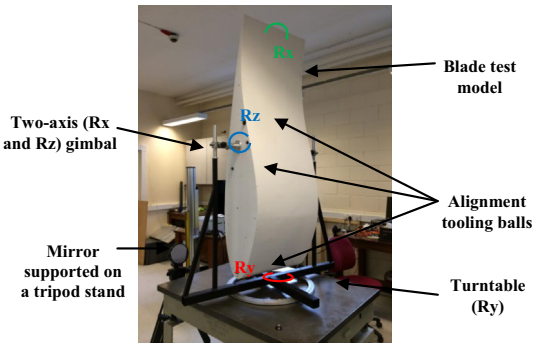

Fig. 9. Blade test model setup within the laboratory. The turntable and gimbal allowed rotation in *Rx*, *Ry* and *Rz*. The mirror provided a line of sight to the underside of the blade and the tooling balls allowed quick alignment to the CAD model.

For results to be reliable, the test model must accurately replicate the CAD model to avoid the generation of artificial results. The test blade was evaluated against the CAD model by measuring the point deviation from the CAD model for three full B-splines evenly separated across the blade face. A tolerance level of ±10 mm was used.

The test model had an average deviation of 4.65 mm from the CAD model, with a range of 12.31 mm. The test model deviated most from the CAD model on the underside of the blade, with an average deviation of 7.22 mm. In addition, 17 points (6.09%) measured did not meet the required tolerance limits.

This shows that the test blade accurately represents the CAD blade model. Artificial results will therefore not be created during data alignment, producing accurate and reliable results for each blade section (front, underside and back).

3.2. Experimental procedure

This investigation used an experimental procedure and data transformation method developed by Nikon. It is commonly implemented on large-scale wind turbine blades and was therefore deemed reliable. Each set of results followed the same experimental procedure, shown in Fig. 10.

1. *Import CAD model into SA:* The test model is imported 5.5 m from the SA coordinate origin as it was designed on a cross-section 5.5 m from the root.
2. *Align CLR scanner to CAD model:* The scanner was aligned to the test model using three tooling balls placed on the root side face shown in Fig. 9. The tooling balls remained in the same location throughout all experiments for quick and accurate alignment.
3. *Construct B-splines and nominal point groups:* B-splines were created to construct nominal point groups, which were used as a reference for the CLR scanner to automatically measure.
4. *Measure nominal point groups:* Nominal point groups were measured in three sections: front, underside and the back. The front was straight-forward to measure;

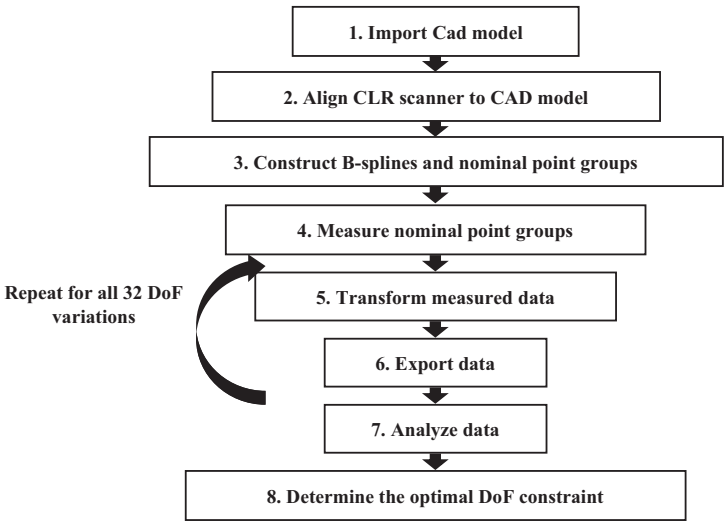

Fig. 10. Experimental procedure used to measure and analyze each constrained DoF variation to establish the optimal data alignment solution.

however a mirror was needed for the underside of the blade. The scanner was relocated for the back of the blade and aligned, adding to the experimental time.

5. *Transform measured data:* The measured data was then fabricated for all 32 DoF constraint variations.
6. *Perform best-fit transformations:* The fabricated data sets were then aligned to their equivalent CLR scanners and transformed to minimize the deviation from the CAD model.
7. *Export data:* All transformed data was exported into an Excel format.
8. *Analyze data:* The mean and standard deviation of distance data between the transformed data sets and the CAD model were calculated within Excel.
9. *Determine the optimal DoF constraint:* The analyzed data for each DoF variation was compared with each other using a ranking system to determine the most accurate transformation of the DoF variations.

This procedure allowed investigation of all 32 DoF variations. A main advantage of this method was that fabricated data sets were used for each DoF variation, requiring only one measurement procedure for each experiment. This saves time and eliminates human error that would be associated with taking multiple measurements. The procedure offers a flexible measurement solution as the number of B-splines and point density can be changed easily in Step 3 above.

To maximize measurement accuracy, care was taken to ensure a controlled laboratory environment was maintained. The CLR scanner and the test model were kept stationary and a clear line of sight between the scanner and blade was preserved, avoiding the need to repeat measurements.

3.3. Data analysis

There were three components of each DoF data alignment transformation that were exported and analyzed:

Surface distance: quantifies the distance between the measured data points and the CAD surfaces. The smallest standard deviation shows the closest alignment towards the CAD surface and proves the most accurate and optimal DoF variation.

Point-to-point distance: quantifies the distance between the measured data points and the equivalent nominal points. The mean point-to-point distance shows how well the transformed data was mapped onto the nominal points; the smallest mean proves the most accurate DoF variation.

Scanner movement: quantifies the notional distance the scanner has moved away from a reference scanner location in order to transform the measured data points.

The reference scanner location is constructed during alignment when the blade is defined as being fully constrained in *X*, *Y*, *Z*, *Rx*, *Ry* and *Rz*. The fully constrained DoF variation data set will therefore always have zero scanner movement and hence the best ranked scanner movement for all experiments.

The smallest mean movement of the scanners proves the most accurate DoF variation.

3.4. Ranking

Each measurement set produced vast amounts of data. The analyzed data therefore required ranking for easy comparison between each DoF variation.

The ranking system ordered each DoF variation in terms of the three data analysis criteria discussed above. The optimal (most accurate) DoF, i.e. the smallest surface vector magnitude, point-to-point distance or scanner movement, was allocated an individual rank score of 1; the least accurate DoF variation an individual rank score of 32.

The individual rank scores were then combined for an overall total rank between 3 and 96 as shown in Fig. 11. The optimal DoF constraint will achieve the lowest total rank score.

Combining the total rank scores across all experiments highlights the DoF variations regularly performing well and therefore the optimal data alignment solution.

3.5. Experimental plan

The experimental procedure, data analysis and ranking above were all used to investigate the 32 DoF variations using a single B-spline and double B-spline arrangements for different *Rx*, *Ry* and *Rz* offsets, simulating blade flex.

A point separation of 50 mm was set for the front and back of the blade and a 12.5 mm separation was used for the underside of the blade. This resulted in 95 nominal inspection points around the blade profile for each B-spline.

The smaller point separation for the underside of the blade reduces the Hausdorff distance, offering greater accuracy than a larger separation. This was necessary as the blade surface turns through 180°.

Experiment 1 – Single B-spline: The single B-spline was defined in SA half-way (250 mm) across the test model, evenly splitting the face as shown in Fig. 12. The B-spline was not constructed near the edge of the test model face as experiment offsets would rotate the blade away from the theoretical B-spline. This would result in failed measurements.

Experiment 2 – Double B-spline: The two B-splines were separated evenly: 166.7 mm and 333.7 mm along the blade face, shown in Fig. 12. Again, the B-spline curves were constructed away from the edge of the blade face.

Using an additional B-spline to Experiment 1 doubles the number of nominal inspection points to190.

Initially, five offsets were chosen using the extreme *Rx*, *Ry* and *Rz* flex simulations for both Experiment 1 and 2: (1) *No Offset; (2) 30° Ry; (3) 20° Rz; (4) 15° Rx; (5) 30° Ry, 20° Rz and 15° Rx.*

3.6. Change in experimental plan

It was found that the initial chosen offsets were not suitable for the experimental method. Implementing offset 1 (no offset) and offset 2 (30° *Ry*) yielded reliable and accurate results. However some results obtained for the 20° *Rz* offset, 15° *Rx* offset and 30° *Ry*, 20° *Rz* and 15° *Rx* offset contained huge inaccuracies shown in Fig. 13.

Fig. 13 shows a huge average point shift of 2124.85 mm and scanner movement of 639.76 mm from the nominal point group. Such a large divergence clearly shows that the CLR method used with SA is incapable of generating reliable results at large offsets simulating extreme blade flex characteristics.

Furthermore, CLR failed to measure numerous nominal points around the profile. However, this was especially true when using the mirror; only 40.7% of points on the underside were measured. This is because large offsets caused the test model to rotate outside the mirror plane.

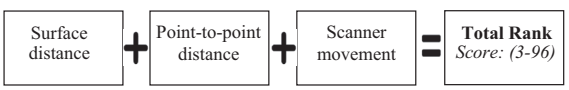

Fig. 11. Summing of the individual rank scores (1–32) from each criterion to give a total rank score (3–96).

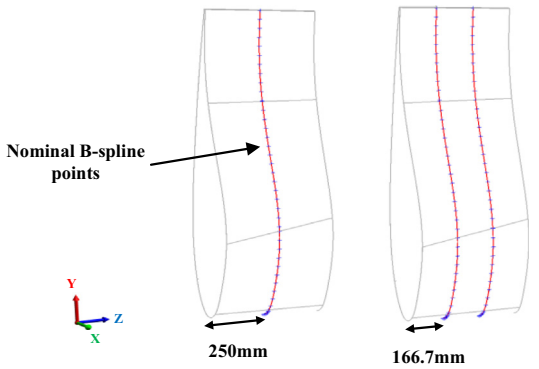

Fig. 12. Left, the single B-spline arrangements (Experiment 1), 250 mm from the root end of the cross-section. Right, the double B-spline arrangement (Experiment 2), evenly distributed 166.7 mm from the root end.

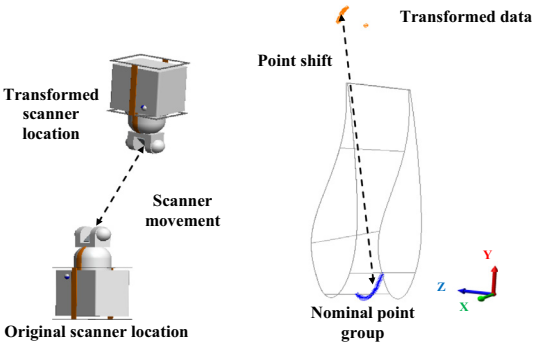

Fig. 13. Huge point shifts and scanner movements were found when implementing a 20° *Rz* offset; the offset was deemed inappropriate.

Different offsets were therefore used simulating a less severe blade flex scenario: (1) *No Offset; (2) 10° Ry; (3) 30° Ry; (4) 5° Rz; (5) 5° Rx; (6) 10° Ry, 5° Rz and 5° Rx.*

Although these offsets are smaller than the initially planned offsets, they still represent a significantly larger blade flex than the common deformation seen during real blade inspection.

The results of this investigation will offer manufacturers confidence in the measurement process, whilst eradicating the measurement inaccuracies associated with large offsets.

The most important experiments to evaluate are Experiments 1.6 and 2.6 as these simulate the most realistic blade flex characteristics that occur during turbine blade testing.

4. Results and analysis

All data is presented in millimetres (mm) and rounded to the nearest 0.01 mm due to the precision of SA point measurement.

4.1. Experiment 1 – Single B-spline

Experiment 1 evaluates all 32 DoF variations for six different *Rx*, *Ry* and *Rz* offsets using a single B-spline.

4.1.1. Experiment 1.1: No offset, simulating the measurement of the blade in its theoretical CAD position with no flex

The results for each DoF constraint variation are displayed showing: the mean point-to-point distance between the measured points and nominal points, the standard deviation of the point distance away from the surface and the mean of the scanner movements from their starting locations. The individual rank scores of each criterion have been summed and displayed as total rank score giving it a rank order compared to the other 32 DoF variations.

Table 1 shows that for Experiment 1.1, the optimal transformational solution is achieved when constraining the blade in either the *Y*, *Z* and *Ry* directions or the *X*, *Z*, *Rx* and *Rz* directions. Both DoF variations achieved the joint lowest total rank score of 26 and therefore have the best data alignment performance when measuring the blade under no deformation (see Tables 2 and 4).

However, there is not much difference in data alignment performance compared with the three DoF variations with a total rank score of 27, which performed almost as well as the two optimal DoF variations. All 10 DoF variations shown in Table 1 have extremely low point-to-point distances and surface distances; however certain DoF variations scored poorly due to large scanner movements of above 75 mm.

4.1.2. Experiment 1.2: A 10° Ry offset, simulating some blade sag

Experiment 1.2 found that the best performing DoF variation is *Y*, *Z* and *Ry* constraints once again, along with *X*, *Z*, *Rx* and *Ry* constraints. The former performed particularly well with a surface distance of 0.69 mm and the latter with no notional scanner movement.

X, *Y*, *Z* and *Rz* constraints also performed well with a total rank score of 20. It had a low surface distance of 0.73 mm.

Comparing Experiments 1.1 and 1.2, it is clear that the introduction of an *Ry* offset simulating blade sag has decreased the accuracy of the data transformation shown by larger point-to-point and surface distances.

4.1.3. Experiment 1.3: A 30° Ry offset, simulating the maximum blade sag scenario

Table 3 shows that the constrained variation of *X*, *Y*, *Z* and *Ry* is the best data alignment technique for maximum blade sag. *X*, *Z* and *Rx* as well as *Z*, *Rx* and *Ry* constrained DoF variations also performed well.

It is clear however that the data alignment transformation is not as accurate for such large sag characteristics compared with the simulation less extreme sag in Experiment 1.2, as shown by greater values for all three criteria.

4.1.4. Experiment 1.4: A 5° Rz offset, simulating some blade twist

The *X*, *Z* and *Rx* constrained DoF variations is the optimal data transformation for Experiment 1.4. Similarly to Experiment 1.3, large values for all 3 criteria were obtained. This is especially true again for the scanner movement with certain movements upwards of 160 mm.

Table 1
Top 10 ranked DoF variations of Experiment 1.1.

DoF constraints	Point-to-point distance	Surface distance	Scanner movement	Total rank score	Rank order
Y Z Ry	1.55	1.40	80.18*	26	1
X Z Rx Rz	1.86	1.81	8.25	26	1
Z Rx Ry	1.53	1.40	83.85*	27	3
Y Z Ry Rz	1.85	1.81	8.62	27	3
Z Rx Ry Rz	1.84	1.81	8.70	27	3
X Y Z Rz	1.88	1.82	8.13	29	6
X Y Z	1.68	1.40	80.24*	30	7
X Z Rx	1.62	1.26	91.10*	30	7
X Z Rx Ry	1.65	1.69	76.72*	31	9
X Y Z Ry Rz	2.57	2.62	6.39	32	10

* Large scanner movements above 75 mm.

Table 2
Top 10 ranked DoF variations of Experiment 1.2.

DoF constraints	Point-to-point distance	Surface distance	Scanner movement	Total rank score	Rank order
Y Z Ry	2.28	0.69	21.44	19	1
X Z Rx Ry	2.47	1.89	0.00	19	1
X Y Z Rz	2.92	0.73	11.69	20	3
Z Rx Ry	2.25	1.84	21.26	23	4
X Z Rx	2.26	1.84	21.42	25	5
X Y Z	2.29	1.84	21.57	29	6
X Z Rx Rz	2.90	2.40	11.77	36	7
X Z Rx Ry Rz	3.52	2.99	7.42	36	7
Y Z Ry Rz	2.90	2.41	12.20	38	9
X Y Z Ry Rz	3.53	2.99	7.48	38	9

Table 3
Top 10 ranked DoF variations of Experiment 1.3.

DoF constraints	Point-to-point distance	Surface distance	Scanner movement	Total rank score	Rank order
X Y Z Ry	8.04	5.01	110.00	24	1
X Z Rx	6.72	5.06	114.11	25	2
Z Rx Ry	6.68	5.08	114.01	25	2
X Z Rx Ry	8.04	4.91	116.67	27	4
Y Z Ry	6.82	5.07	114.75	28	5
Z Rx Ry Rz	11.58	10.11	32.49	30	6
X Z Rx Rz	11.63	10.11	31.68	31	7
X Y Z Rz	11.68	10.12	31.46	33	8
Z Rx	55.59	4.69	77.94	34	9
Y Z Ry Rz	11.62	10.12	32.59	34	9

Table 4
Top 10 ranked DoF variations of Experiment 1.4.

DoF constraints	Point-to-point distance	Surface distance	Scanner movement	Total rank score	Rank order
X Z Rx	7.25	6.14	161.77	24	1
Z Rx Ry	7.13	6.18	161.77	27	2
Z Rx	14.13	6.20	102.88	30	3
Y Z Ry	7.39	6.16	161.96	30	3
X Y Z	7.37	6.18	162.22	32	5
X Z Rx Ry	10.99	6.75	124.29	32	5
Y Z	15.93	6.31	105.74	33	7
X Y Z Ry	10.92	6.80	164.11	40	8
X Z Ry Rz	21.60	21.33	0.00	41	9
X Z Rx Rz	21.65	21.15	54.94	43	10

4.1.5. Experiment 1.5: A 5° Rx offset, simulating some blade twist

Table 5 shows that the optimal DoF variation for a small *Rx* offset is when *Y*, *Z* and *Ry* are constrained. However there is not much difference in the three analysis criteria for the top three ranked DoF variations shown by a range of: 0.05 mm, 0.02 mm and 1.46 mm for the point-to-point distance, surface distance and scanner movement respectively.

4.1.6. Experiment 1.6: A 10° Ry, 5°Rz and 5° Rx offset, simulating the most realistic blade flex scenario during testing; sag and twist

Experiment 1.6 is a combination of Experiments 1.2, 1.4 and 1.5 and best simulates the blade in a real test environment. Interestingly, Experiment 1.6 suggests that the optimal data alignment is achieved when constraining *Y* and *Z*.

This was not expected as the *Y* and *Z* constrained variation did not perform well in previous experiments.

Y, *Z* and *Ry* constrained and *Z*, *Rx* and *Ry* constrained DoF variation also performed strongly, both ranking second.

Due to the large offset however, large values for each criterion were obtained: above 20 mm, 16 mm and 100 mm for point-to-point distance, surface distance and scanner movement respectively (see Table 6).

4.2. Experiment 2 – Double B-spline

Experiment 2 evaluates all 32 DoF variations for the same *Rx*, *Ry* and *Rz* offsets as in Experiment 1 using a double B-spline.

4.2.1. Experiment 2.1: No offset, simulating the measurement of the blade in its theoretical CAD position with no flex

Table 7 shows the strong performing data alignment DoF variations without any blade deformation. Similar to Experiment 1.1, both *Y*, *Z* and *Ry* constrained and *Z*, *Rx* and *Ry* constrained DoF variations performed very well along with *X*, *Z* and *Rx* constrained and *X*, *Y* and *Z* constrained.

The lower total rank scores (18) to that of the equivalent investigation (26) in Experiment 1.1 show that the DoF variations are performing more consistently with the criteria categories. This is due to less extreme scanner movements of ~15 mm against ~80 mm in Experiment 1.1.

Table 5
Top 10 ranked DoF variations of Experiment 1.5.

DoF constraints	Point-to-point distance	Surface distance	Scanner movement	Total rank score	Rank order
Y Z Ry	4.93	5.04	23.51	16	1
X Y Z	4.97	5.06	22.15	18	2
X Z Rx	4.98	5.06	22.19	20	3
Y Z Rx	5.23	3.81	24.27	20	3
Z Rx Ry	4.94	5.04	27.20	23	5
X Z Rx Rz	5.84	5.87	0.00	28	6
X Y Z Rx	5.26	5.51	26.50	30	7
Y Z Rx Ry	5.26	5.50	29.22	35	8
Z Rx Ry Rz	5.82	5.86	26.75	37	9
Y Z Ry Rz	5.82	5.87	26.79	39	10

Table 6
Top 10 ranked DoF variations of Experiment 1.6.

DoF constraints	Point-to-point distance	Surface distance	Scanner movement	Total rank score	Rank order
Y Z	7.92	6.12	138.34	27	1
Y Z Ry	8.15	6.10	147.12	30	2
Z Rx Ry	21.35	5.84	111.20	30	2
X Z Rz	22.18	23.18	0.00	31	4
Z Ry Rz	22.18	23.18	0.00	31	4
X Z Rx	7.98	6.15	147.25	32	6
Y Z Rx	20.79	16.88	61.76	32	6
X Y Z Ry	11.11	7.28	132.01	35	8
X Z Rx Ry	11.24	6.90	141.44	37	9
X Y Z	8.22	6.15	251.73	42	10

4.2.2. Experiment 2.2: A 10° Ry offset, simulating some blade sag

Table 8 shows that *Z*, *Rx* and *Ry* constrained DoF variation achieved the highest rank for Experiment 2.2. However, there was not much difference in performance with the other high ranking DoF constraint variations.

The data alignment transformations performed poorly due to the point-to-point distance criterion. The *Z*, *Rx* and *Ry* constrained variation achieved a point-to-point distance of 23.02 mm for the double B-spline arrangement compared with 2.25 mm for a single B-spline in Experiment 1.2.

4.2.3. Experiment 2.3: A 30° Ry offset, simulating the maximum blade sag scenario

The larger rotational offset in *Ry* limited the ability of CLR to measure certain points in this particular configuration. Only three points from 28 (10.7%) from the underside of the test model were measured for one of the B-splines. As mentioned in 'Theory: C. Spatial Analyzer', SA requires four or more data points to significantly improve the accuracy of the best-fit transformation.

This is the reason scanner movements as large as 506.33 mm were obtained. A 30° *Ry* offset was therefore deemed inappropriate for the double B-spline arrangement.

4.2.4. Experiment 2.4: A 5° Rz offset, simulating some blade twist

Table 9 shows that *Y*, *Z* and *Ry* constrained and *Z*, *Rx* and *Ry* constrained DoF variations are the best data alignment

Table 7
Top 10 ranked DoF variations of Experiment 2.1.

DoF constraints	Point-to-point distance	Surface distance	Scanner movement	Total rank score	Rank order
X Z Rx	1.55	1.43	15.28	18	1
Y Z Ry	1.55	1.42	15.87	18	1
Z Rx Ry	1.53	1.42	15.95	18	1
X Y Z	1.57	1.43	15.15	19	4
X Z Rx Rz	1.89	1.87	9.49	23	5
Y Z Ry Rz	1.88	1.87	9.90	23	5
Z Rx Ry Rz	1.87	1.87	9.98	23	5
X Y Z Rz	1.90	1.88	9.33	28	8
Z Rx Rz	2.39	1.87	14.11	31	9
X Z Rx Ry Rz	2.61	2.70	4.16	33	10

Table 8
Top 10 ranked DoF variations of Experiment 2.2.

DoF constraints	Point-to-point distance	Surface distance	Scanner movement	Total rank score	Rank order
Z Rx Ry	23.02	3.30	39.57	27	1
Y Z	11.74	2.37	70.09	28	2
Y Z Ry	23.08	3.30	39.93	29	3
Z Rx Ry Rz	23.93	3.82	19.51	30	4
Z Rx	14.52	2.24	72.98	31	5
Y Z Ry Rz	23.94	3.80	19.77	31	5
Z Rx Rz	12.76	4.18	40.96	34	7
X Y Z Ry Rz	24.75	4.08	15.74	34	7
X Z Rx Ry Rz	24.73	4.08	15.96	34	7
Y Z Rz	13.73	4.16	44.27	36	10

transformations. However, large scanner movements and some large point-to-point and surface distances can be seen for other DoF variations.

4.2.5. Experiment 2.5: A 5° Rx offset, simulating some blade twist

Table 10 shows that fully constrained in *X*, *Y*, *Z*, *Rx*, *Ry* and *Rz* is the optimal data alignment DoF variation for a 5° *Rx* offset. No notional scanner movement was seen because the scanner reference is predefined using a fully constrained configuration. Although a low surface distance of 2.50 mm was observed, a huge point-to-point distance of 26.70 mm was obtained; it is therefore performing inconsistently across the three analysis criteria (see Table 11).

4.2.6. Experiment 2.6: A 10° Ry, 5° Rz and 5° Rx offset, simulating the most realistic blade flex scenario during testing; sag and twist

Similar to Experiment 1.6, *Y*, *Z* and *Ry* constrained and *Z*, *Rx* and *Ry* constrained DoF variations performed well, ranking in joint second along with the *Z* and *Rx* constrained variation. However, the top ranking variation was the *X*, *Z* and *Rx* constraint, slightly outperforming those ranked second.

The large values observed for all three criteria for most DoF variations are due to the large offset simulating significant blade flex.

Table 9
Top 10 ranked DoF variations of Experiment 2.4.

DoF constraints	Point-to-point distance	Surface distance	Scanner movement	Total rank score	Rank order
Y Z Ry	6.76	4.89	125.62	27	1
Z Rx Ry	6.52	4.92	125.39	27	1
Y Z	17.72	4.75	114.35	29	3
X Z Rx	6.60	4.90	130.43	29	3
X Y Z	6.78	4.93	130.65	34	5
X Z Ry	11.10	7.08	117.41	36	6
X Z Rx Ry	9.72	5.82	134.97	38	7
X Y Z Ry	9.82	6.00	139.67	41	8
X Z Rx Rz	19.84	21.00	59.37	42	9
Z Rx Ry Rz	19.82	21.00	62.45	42	9

5. Discussion

5.1. Single B-spline arrangement

The optimal data alignment transformation using one B-spline was achieved when constraining in *Y*, *Z* and *Ry* DoF whilst keeping *X*, *Rx* and *Rz* unconstrained. This DoF variation was ranked first for Experiments 1.1, 1.2 and 1.5 and achieved the lowest total rank score across all six offset scenarios. Averaged across the six offsets, the constraint obtained a low point-to-point and surface distance of 5.19 mm and 4.08 mm respectively, however it achieved a large scanner movement of 91.49 mm.

The *Z*, *Rx* and *Ry* constrained DoF variation ranked second overall. Compared with the *Y*, *Z* and *Ry* constraint, the variation achieved a higher average point-to-point and surface distance of 7.31 mm and 4.23 mm respectively; however it outperformed the *Y*, *Z* and *Ry* DoF constraint with an average scanner movement of 86.55 mm.

There is no apparent relationship between the number of constrained DoF and data alignment performance; however four of the top five DoF variations imposed *Ry* constraints. Constraining in the *X* direction also appears to increase the accuracy of the alignment transformation with six of the top ten variations using *X* constraints.

CLR was capable of measuring the majority of points along the B-spline with Experiments 1.1–1.5 achieving point measurement success percentages of above 90%. Experiment 1.6 achieved 84.21% measurement success which still ensures reliable results.

The large scanner movements observed when using a single B-spline could introduce significant errors when defining a general coordinate system when combining multiple CLR scanners in the six locations needed to measure a 60 m blade.

CLR has a very short measurement time for a single B-spline arrangement, measuring 95 points in ~6 min. The entire process however, including mirror alignment and results fabrication, is time-consuming: a full set of results can take up to 6 h to complete. In reality, mirror positioning would not be done by hand and multiple B-splines would be measured for each scanner location, saving a considerable amount of time.

Therefore, for a single B-spline arrangement, the best-fit data alignment transformation should be implemented

Table 10
Top 10 ranked DoF variations of Experiment 2.5.

DoF constraints	Point-to-point distance	Surface distance	Scanner movement	Total rank score	Rank order
X Y Z Rx Ry Rz	26.70	2.50	0.00	23	1
X Z Rx	4.16	4.53	15.86	24	2
X Y Z Rx	4.41	4.91	11.73	25	3
Y Z Ry	5.11	4.51	15.89	27	4
X Y Z	4.14	4.52	39.87	28	5
X Y Z Rz	4.92	5.46	5.49	28	5
X Z Rx Rz	4.92	5.46	5.49	28	5
Z Rx Ry	5.16	4.54	14.65	29	8
Y Z Rx Ry	5.43	4.93	12.55	32	9
Y Z Rx	10.89	4.50	34.97	36	10

Table 11
Top 10 ranked DoF variations of Experiment 2.6.

DoF constraints	Point-to-point distance	Surface distance	Scanner movement	Total rank score	Rank order
X Z Rx	8.20	6.20	140.97	27	1
Z Rx	13.10	6.17	120.60	28	2
Y Z Ry	8.31	6.23	140.76	28	2
Z Rx Ry	8.07	6.21	141.00	28	2
X Y Z	8.43	6.23	140.95	30	5
Y Z	12.64	6.26	139.18	33	6
Z Ry Rz	21.39	22.38	12.72	33	6
X Y Z Rz	19.27	20.17	87.95	37	8
X Z Rx Ry	11.52	7.26	145.13	37	8
X Y Z Ry	11.75	7.80	160.76	40	10

with constraints in *Y*, *Z* and *Ry*, offering a simple, quick and accurate large-scale measurement method. However, care must be taken when aligning multiple CLR scanners.

5.2. Double B-spline arrangement

Similarly to the single B-spline, the most accurate data alignment solution for a double B-spline arrangement was found with *Y*, *Z* and *Ry* constrained DoF. This DoF variation ranked first for Experiments 2.1 and 2.4 and ranked in the top four for all offsets. Again, it achieved the lowest combined total rank score across the different offsets. The data alignment solution had an average point-to-point distance of 8.96 mm, a surface distance average of 4.07 mm and a scanner movement of 67.61 mm.

Once again, the *Z*, *Rx* and *Ry* constraint also performed strongly; ranking second with an average point-to-point distance of 8.86 mm, an average surface distance of 4.08 mm and an average scanner movement of 67.31 mm.

No clear relationships between constraints and results can be seen. However, the variations with fewer constrained DoF generally rank poorly due to large scanner movements.

The addition of a second B-spline did not affect the measurement capability of CLR. CLR achieved similar point measurement success (excluding Experiment 2.3) to that of the single B-spline data alignment, with an average of 89.6% of nominal points measured across the different offsets. Experiment 2.3 achieved a measurement success percentage of 60% resulting in a less accurate transformation.

When using a double B-spline arrangement, it is recommended to use the best-fit data alignment transformation constrained in *Y*, *Z* and *Ry*. The addition of a second B-spline doubled the experimental time to up to 12 h; this would only increase further with more B-splines.

5.3. Comparison of single and double B-spline arrangements

The optimal data alignment transformation for both the single and double B-spline arrangements were achieved with *Y*, *Z* and *Ry* constrained DoF.

For the *Y*, *Z* and *Ry* constrained DoF, the double B-spline data alignment had no effect on the average surface distance across all flex offsets.

However, the average point-to-point distance was less accurate; 8.96 mm compared with 5.19 mm with the single B-spline. This is due to the single B-spline being constructed along the *Y* axis (situated in the centre of the blade cross-section) shown in Fig. 12. The blade rotates around the single B-spline when simulating sag with a rotational offset in *Ry*, as investigated in Experiments 1.2, 1.3 and 1.6 and for the equivalent in Experiment 2. Points measured along the B-spline will therefore be less affected by the offset than points away from the centre of rotation (such as points along the double B-splines) because the initial measured point-to-point distances are greater.

This is also the reason why some nominal point measurements failed when using the mirror for the double B-spline. Points on the underside of the blade rotated outside of the mirror's line of sight whereas the single B-spline points did not rotate through a large angle and therefore remained in view.

Interestingly, the double B-spline achieved a smaller average scanner movement (67.61 mm) than that seen with the single B-spline (91.49 mm). This reduces the potential error that could be introduced when aligning a new scanner location in SA.

Similar comparisons, between the single and double B-spline data alignments can be made with other DoF variations. However, other DoF variations, including the *Z*, *Rx* and *Ry* constraint achieved more accurate surface distance results for the double B-spline arrangement. The surface distance for the *Z*, *Rx* and *Ry* constrained DoF decreased from 4.23 mm for the single B-spline to 4.08 mm for the double B-spline.

Although the inspection time is twice as long as a single B-spline, it is recommended that a double B-spline data alignment method should be implemented with *Y*, *Z* and *Ry* constrained DoF. The double B-spline achieved more accurate results with a slight decrease in point distance away from the CAD surface and a significant decrease in scanner movement. Although the average point-to-point distance increased, this may have been due to inaccuracies associated with the offset rotation in the *Y* axis. The large *Ry* offsets also cause some point measurement failure. In reality, blade flex is small, meaning nominal points will be measured consistently.

5.4. Experimental evaluation and recommendations

The accuracy of results obtained in this investigation relies heavily on the closeness of the measurement data to the real data of the product. It was found that the blade test model accurately represented the CAD model; certain parts of the blade did not meet with tolerance limits. This would have a slight negative effect on measurement accuracy. If possible, the data alignment method should be applied to a test model that more accurately represents the CAD blade profile (particularly the underside of the blade).

B-splines were defined to evenly separate the blade meaning the single B-spline was positioned halfway across (i.e. the centre) of the blade face, along the *Y* axis. This meant an accurate comparison between the single and double B-splines could not be made when offset in *Ry*. The single B-spline should be tested in a location away from the *Ry* axis to enable a better comparison with double B-spline results.

This investigation showed that the double B-spline was more accurate than the single B-spline averaged across all offsets. Therefore, a triple B-spline arrangement should be investigated to examine what effect further increasing the number of B-splines has on the accuracy of results.

Due to the small mirror size, the mirror was unable to measure a proportion of points when simulating large blade flex characteristics as the nominal points were offset to beyond the mirror's line of sight. A larger mirror would increase the number of points that CLR was able to measure. However a bigger mirror may be expensive and less accurate.

In the future, similar investigations should be performed on a real large-scale wind turbine blade to validate results found in this piece of research.

6. Conclusion

This investigation found that although accurate, the data alignment technique currently used by Nikon (*Z*, *Rx* and *Ry* constraints) can be improved. The constrained DoF combination of *Y*, *Z* and *Ry* (allowing movement in *X*, *Rx* and *Rz*) for a double B-spline arrangement delivered the optimal transformation solution. It was the most accurate and consistent performing DoF variation; minimizing the measurement error introduced by blade flex characteristics.

It was found that using the double B-spline arrangement increased data post-processing accuracy. Therefore, using more B-spline curves during blade inspection reduces the overall measurement error.

Additionally, it was found that the mirror increased measurement accuracy by 29.70% for parts of the underside of the blade where CLR could not accurately focus due to a large incidence angle. However, the number of nominal points the mirror could measure decreased with greater blade flex.

The proposed data alignment solution offers a simple, quick and accurate measurement solution, minimizing measurement error during inspection. This provides manufacturers with confidence in their manufacturing procedures. The techniques described in this paper can easily be developed and used for the metrology of other large-scale structures.

Acknowledgments

This research is part of the wind turbine structural condition monitoring program funded by EPSRC, United Kingdom, through the Centre for Through Life Engineering Services (EP/1033246/1, Project SC006) and EPSRC Impact Acceleration Award (EP/K50336811).

References

[1] Digest of the United Kingdom energy statistics (DUKES), Renewable sources of energy, 2013 (Chapter 6), Available: <https://www.gov.uk/government/uploads/system/uploads/attachment_data/file/65850/DUKES_2013_Chapter_6.pdf>.
[2] Gurit, Wind turbine blade structural engineering, Wind Energy Handbook – 3 – Structural Design.
[3] Gurit, Gurit materials for wind turbine blades, Wind Energy Handbook – 4 – Gurit Composite Materials for Wind Turbine Blades.
[4] M.A. Homel, Blade Geometry and Solid Models, 2005, Available: <http://www.mech.utah.edu/senior_design/05/index.php/WindTurbine/MikeGroupReport>.
[5] Quality Digest, Metris, Laser radar supports engineering of wind turbine blade aerodynamics, 2009, Available: <http://www.qualitydigest.com/inside/twitter-ed/laser-radar-supports-engineering-wind-turbine-blade-aerodynamics.html>.
[6] A. Summers, Investigating the measurement of offshore wind turbine blades using coherent laser radar, MEng Technical Report, Durham University, April 2013.
[7] G.N. Peggs et al., Recent developments in large-scale dimensional metrology, Proc. Inst. Mech. Eng., Part B: J. Eng. Manuf. 223 (B6) (2008) 571–595.
[8] D.A. White, Quality Digest, Coherent Laser Radar: True Noncontact 3-D Measurement Has Arrived, 1999, Available: <http://www.qualitydigest.com/aug99/html/body_radar.html>.
[9] Nikon, High-Accuracy Bridge CMM, 2014, Available: <http://www.nikonmetrology.com/en_EU/Products/Coordinate-Measuring-Machines/Bridge-CMM/High-Accuracy-Bridge-CMM/(specifications)>.
[10] K.H. Lee, H. Woo, T. Suk, Data reduction methods for reverse engineering, Int. J. Adv. Manuf. Technol. 17 (10) (2001) 735–743.
[11] B.L. Curless, New Methods for Surface Reconstruction from Range Images, PhD Dissertation, Stanford University, 1997.
[12] Quality Digest, Study: Comparison Between Photogrammetry and Laser Radar, 2010, Available: <http://www.qualitydigest.com/inside/cmsc-article/study-comparison-between-photogrammetry-and-laser-radar.html#>.
[13] Nikon, MV330/MV350 Laser Radar, 2014, Available: <http://www.nikonmetrology.com/en_EU/Products/Large-Volume-Applications/Laser-Radar/MV330-MV350-Laser-Radar/(key_features)>.
[14] O.E. DeLange, Optical heterodyne detection, Spectrum, IEEE 5 (10) (1968) 77–85.
[15] W.T. Estler, K.L. Edmundson, G.N. Peggs, D.H. Parker, Large-scale metrology – an update, CIRP Ann. – Manuf. Technol. 51 (2) (2002) 587–609.
[16] Nikon, Laser Radar MV330/350 Automated Large Volume Inspection, 2010, Available: <http://www.smart-solutions.pl/download/laser-radar-mv330.pdf>.
[17] Q. Wang, N. Zissler, R. Holden, Evaluate error sources and uncertainty in large scale measurement systems, Robot. Comput.-Integr. Manuf. 29 (1) (2013) 1–11.
[18] Laser Beam Products, Mirror Coatings: Protected Aluminium, 2014, Available: <http://www.lbp.co.uk/pdfs/pdf_files/coatings.pdf>.
[19] C.J. Brochu, J.W. Moffat, G.A. Morin, Optical Alignment of the Spherical Antenna Measurement System, Defence Research Establishment Ottawa, 1997.
[20] J.H. Burge, P. Su, C. Zhao, T. Zobrist, Use of a commercial laser tracker for optical alignment, Opt. Syst. Alignment Toleranc. 6676 (2007).
[21] R.P Elliott, Quality Digest, Measurement Accuracy of a Mirrored Surface Using a Laser Tracker, 2013, Available: <https://www.qualitydigest.com/inside/cmsc-article/measurement-accuracy-mirrored-surface-using-laser-tracker.html#>.
[22] New River Kinematics, SpatialAnalyzer®: Features & Benefits, 2014, Available: <http://www.kinematics.com/spatialanalyzer/features.php>.
[23] New River Kinematics, SpatialAnalyzer®: Unified Spatial Metrology Network (USMN), 2014, Available: <http://www.kinematics.com/spatialanalyzer/usmn.php>.
[24] Joint Committee for Guides in Metrology (JCGM/WG 1), Evaluation of Measurement Data – Guide to the Expression of Uncertainty in Measurement, 2008.
[25] J.M. Calkins, Quantifying Coordinate Uncertainty Fields in Coupled Spatial Measurement Systems, PhD Dissertation, Virginia Polytechnic Institute and State University, 2002.
[26] N.M. Patrikalakis, T. Maekawa, W. Cho, Shape Interrogation for Computer Aided Design and Manufacturing, Hyperbook Edition, 2009, Available: <http://web.mit.edu/hyperbook/Patrikalakis-Maekawa-Cho/node12.html>.
[27] E. Savio, L. De Chiffre, R. Schmitt, Metrology of freeform shaped parts, Ann. CIRP 56 (2007).
[28] C.D. Boor, On calculating with B-splines, J. Approx. Theory 6 (1970) 50–62.
[29] J. Chen, G.-J. Wang, Approximate merging of B-spline curves and surfaces, Appl. Math. – A J. Chin. Univ. (2010).
[30] X.-D. Chen, W. Ma, G. Xu, J.-C. Paul, Computing the Hausdorff distance between two B-spline curves, Comput.-Aided Des. 42 (2010) 1197–1206.